



# Elongational viscosity of poly(propylene carbonate) melts: tube-based modelling and primitive chain network simulations

Manfred H. Wagner<sup>1</sup> · Esmail Narimissa<sup>2,3</sup> · Yuichi Masubuchi<sup>4</sup>

Received: 8 August 2022 / Revised: 11 October 2022 / Accepted: 11 October 2022 / Published online: 12 November 2022  
© The Author(s) 2022

## Abstract

In fast elongational flows, linear polymer melts exhibit a monotonic decrease of the viscosity with increasing strain rate, even beyond the contraction rate of the polymer defined by the Rouse time. We consider two possible explanations of this phenomenon: (a) the reduction of monomeric friction and (b) the reduction of the tube diameter with increasing deformation leading to an Enhanced Relaxation of Stretch (ERS) on smaller length scales. (Masubuchi et al. (2022) reported Primitive Chain Network (PCN) simulations using an empirical friction reduction model depending on segmental orientation and could reproduce the elongational viscosity data of three poly(propylene carbonate) melts and a polystyrene melt. Here, we show that the mesoscopic tube-based ESR model (Wagner and Narimissa 2021) provides quantitative agreement with the same data set based exclusively on the linear-viscoelastic characterization and the Rouse time. From the ERS model, a parameter-free universal relation of monomeric friction reduction as a function of segmental stretch can be derived. PCN simulations using this friction reduction relation are shown to reproduce quantitatively the experimental data even without any fitting parameter. The comparison with results of the earlier PCN simulation results with friction depending on segmental orientation demonstrates that the two friction relations examined work equally well which implies that the physical mechanisms of friction reduction are still open for discussion.

**Keywords** Entangled polymers · Elongational flows · Polymer dynamics · Molecular simulations · Constitutive equations

## Introduction

The tube model of Doi and Edwards (Doi and Edwards 1978a,b, 1979) predicts universal rheological behaviour in both the linear and the non-linear viscoelastic regimes for

entangled melts and solutions of linear polymers. While experimental data support universality of the linear viscoelasticity of polymer systems depending on only three material parameters as specified by plateau modulus, characteristic time, and number of entanglements (see e.g. Huang et al. 2013a,b), universality fails in the non-linear viscoelastic regime as especially evident in elongational flow: The Doi-Edwards model expects a monotonic decrease of the elongational viscosity  $\eta_E$  approaching a scaling of  $\eta_E \propto \dot{\epsilon}^{-1}$ , followed by a sudden increase when chain stretch becomes important at strain rates  $\dot{\epsilon}$  larger than the inverse of the Rouse time  $\tau_R$ . While this behaviour was found at least qualitatively for polystyrene solutions (Huang et al. 2013a,b, 2016) and a poly(n-butyl acrylate) (PnBA) melt (Bhattacharjee et al. 2002, 2003; Ye et al. 2003), the seminal experiments by Bach et al. (2003a,b) showed that the elongational viscosity  $\eta_E$  of polystyrene melts decreases monotonously even at strain rates  $\dot{\epsilon} \gg \tau_R^{-1}$  with a scaling approaching  $\eta_E \propto \dot{\epsilon}^{-1/2}$ .

These experimental findings demonstrate that the non-linear viscoelasticity of entangled polymeric liquids is not universal as expected by the Doi-Edwards model, but

✉ Manfred H. Wagner  
manfred.wagner@tu-berlin.de

✉ Yuichi Masubuchi  
mas@mp.pse.nagoya-u.ac.jp

<sup>1</sup> Polymer Engineering/Polymer Physics, Berlin Institute of Technology (TU Berlin), Ernst-Reuter-Platz 1, 10587 Berlin, Germany

<sup>2</sup> Department of Chemical Engineering, Technion–Israel Institute of Technology (IIT), 32 000 Technion City, Haifa, Israel

<sup>3</sup> Department of Chemical Engineering, Guangdong Technion–Israel Institute of Technology (GTIIT), Shantou 515063, China

<sup>4</sup> Department of Materials Physics, Nagoya University, Nagoya 4648603, Japan

seems to be chemistry dependent, and a number of theoretical explanations have been proposed. According to two recent reviews (Ianniruberto et al. 2020; Matsumiya and Watanabe 2021), one explanation is the possible reduction of segmental friction of highly oriented polymer chains in melts under fast extensional flow, as proposed by Ianniruberto et al. (2011, 2012). This concept was supported by primitive chain network (PCN) (Yaoita et al. 2012) and non-equilibrium molecular dynamics (NEMD) simulations (Masubuchi et al. 2013, 2014a, b; Ianniruberto and Marrucci 2020). The magnitude of friction reduction depends on the chemistry of the polymer and diminishes with decreasing polymer concentration in solution resulting in the non-universality of the elongational rheology of polymer melts and solutions (Masubuchi et al. 2014b; Wingstrand et al. 2015; Huang et al. 2015). Recently, Masubuchi et al. (2022) used primitive chain network simulations with and without monomeric friction reduction to analyse the elongational viscosity of poly(propylene carbonate) (PPC) melts. While PCN simulations with constant monomeric friction overestimated the elongational viscosity greatly, they found good agreement between experimental data and simulations if friction was assumed to decrease with increasing segmental orientation. To investigate the effect of chemistry, Masubuchi et al. (2022) also conducted PCN simulations for a polystyrene (PS) melt, which has a similar number of entanglements per chain and a similar polydispersity index as one of the PPC melts investigated. They reported that PPC and PS behave similarly in terms of reduction of friction under fast elongational flow, and no chemistry effect was found.

However, we remark that so far the effect of friction reduction is modelled by use of empirical functions related to segmental orientation or elongational stress with parameters fitted to experimental data of elongational viscosity, and the specific physical parameters determining friction reduction are still unclear. An alternative concept to account for the non-universality of non-linear viscoelasticity is based on the reassessment of the assumption of constant tube diameter in the classical Doi-Edwards model. As shown by Doi and Edwards (1978a) themselves, the line density, i.e., the number of Kuhn monomers that are found per length of the tube, is a well-defined thermodynamic quantity that characterizes the tube diameter. When stretching the polymer chain by non-linear deformation, the line density will necessarily decrease and in the mesoscopic context of the tube model, this will result in a tube diameter decreasing from its equilibrium value with increasing deformation. Within this concept of tube models with varying tube diameter, Marrucci and Ianniruberto (2004) suggested an interchain pressure (IP) model to explain the extension thinning found in elongational flow of polymer melts at strain rates above the inverse Rouse time. Based on the IP model, Wagner et al. (2005) developed an extended interchain pressure (EIP) model and identified the tube diameter relaxation time

proposed by Marrucci and Ianniruberto as the Rouse stretch relaxation time. Narimissa et al. (2020a,b) extended the EIP model by taking the dependence of the interchain tube pressure effect on polymer concentration and molar mass of oligomeric solvents into account and demonstrated good agreement between model predictions and the elongational viscosity data of polystyrene melts and solutions (Wagner and Narimissa 2021; Wagner et al. 2021a,b).

Recently, an enhanced relaxation of stretch (ERS) model was proposed by Wagner and Narimissa (2021), which is also based on the concept of tube diameter reduction and which starts directly from the definition of the Rouse time being proportional to the square of the number of monomers in the chain. They considered a control volume of diameter and length  $a$  representing the decreasing tube diameter with increasing deformation. The number of monomers in this control volume decreases with deformation with the consequence of enhanced relaxation of stretch (ERS) on smaller length scales. In spite of the different constitutive assumptions, the ERS model leads to nearly identical predictions of the elongational viscosity of polystyrene melts and solutions as the EIP model, and to a quantitative agreement with experimental elongational viscosity data based exclusively on the LVE characterization and the Rouse time of the polymer systems considered. Wagner and Narimissa (2021) also showed that the ERS model can be converted into an equivalent Rouse stretch-relaxation model with monomeric friction reduction, resulting in a parameter-free universal relation of monomeric friction reduction as a function of stretch. In this way, a direct comparison with the corresponding empirical expressions of monomeric friction reduction used so far in primitive chain network (PCN) simulations and non-equilibrium molecular dynamics (NEMD) simulations was possible, and at least qualitative agreement was found.

This article intends to present a direct comparison between predictions of the ERS model and primitive chain network (PCN) simulations based on the parameter-free relation of monomeric friction reduction, as derived from the ERS model. The article is organized as follows: We first give a short report on the experimental data and the linear-viscoelastic characterization of the polymer systems considered, followed by a short summary of the ERS model and a comparison to the experimental data of PPC and PS melts. We then present the basics of the PCN simulations and the resulting predictions, followed by discussion and conclusions.

## Experimental data and linear-viscoelastic characterization

Table 1 presents the samples examined in this study. The experimental data of three PPC samples having different molecular weights with relatively narrow molecular weight

distributions are considered, and their molecular characterization has been reported previously (Yang et al. 2021, 2022). All of them were prepared by precipitation fractionation of a commercial PPC. The absolute molecular weight was determined by multi-angle light scattering (MALS). The samples are coded according to  $M_w$  (in kg/mol) obtained by MALS. In addition, we compare the data for the PPC samples with a PS sample reported in the literature (Yang et al. 2022). The molecular characteristics of the PS sample (PS520k) are also shown in Table 1.

Small amplitude oscillatory shear (SAOS) measurements were performed by MCR301 (Anton-Paar) rheometer with a strain of 1%. A parallel plate with a diameter

of 8 mm was used with a gap value of 1 mm. Angular frequencies  $\omega$  of 0.1–100 rad/s were applied at the temperature ranging from 60 to 140 °C. Master curves of storage and loss modulus,  $G'$  and  $G''$ , were obtained by the time–temperature superposition (TTS) at the reference temperature  $T_r$  (70 °C for the PPC melts and 130 °C for the PS melt) and are shown in Fig. 1. Elongational measurements were performed with a filament-stretching rheometer, VADER1000, Rheo Filament (Huang et al. 2016) and are shown in Figures 2 and 5. For PPC69k and PPC111k, elongational viscosities were measured at 70 °C, while for PPC158k elongational viscosities were measured both at 70 °C and 100 °C, and the data at 100 °C were time–temperature shifted to 70 °C. For details, see Yang et al. (2022).

We fitted the mastercurves of  $G'$  and  $G''$  here by parsimonious relaxation spectra for characterization of the linear-viscoelastic relaxation modulus  $G(t)$ ,

$$G(t) = \sum_{i=1} g_i \exp(-t/\tau_i) \tag{1}$$

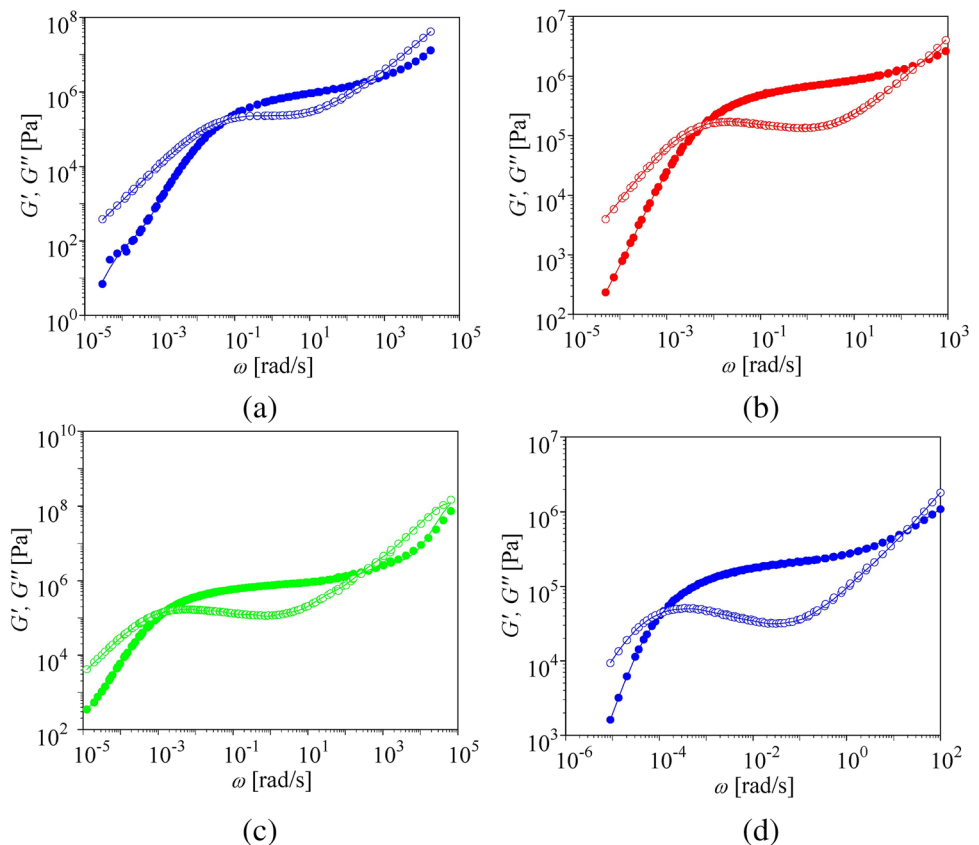
The partial moduli  $g_i$  and relaxation times  $\tau_i$  (Table 2), as determined by the IRIS software (Winter and Mours 2006; Poh et al. 2022) result in excellent agreement with the linear-viscoelastic data of  $G'$  and  $G''$ , see Fig. 1.

**Table 1** Sample characterization

Characteristics	PPC69k	PPC111k	PPC158k	PS520k
$M_w$ [kg/mol]	68.8	111	158	520
$M_w/M_n$	1.43	1.30	1.31	1.3
$T_r$ [°C]	70	70	70	130
$G_N$ [MPa]	0.67	0.67	0.67	0.22
$\eta_0$ [Pa·s]	8.80e+6*	8.64e+7	3.50e+8	1.12e+9
$\tau_d$ [s]	559*	1579	11,372	22,513
$\tau_R$ [s]	2.97*	15.0	37.0	396

\*TTS shifted by  $a_T=0.7$

**Fig. 1** Storage ( $G'$ ) and loss modulus ( $G''$ ) of PPC69k (a), PPC111k (b), and PPC158k (c) at  $T=70$  °C, and PS520k (d) at  $T=130$  °C. Lines are fit by parsimonious spectra (Table 2)



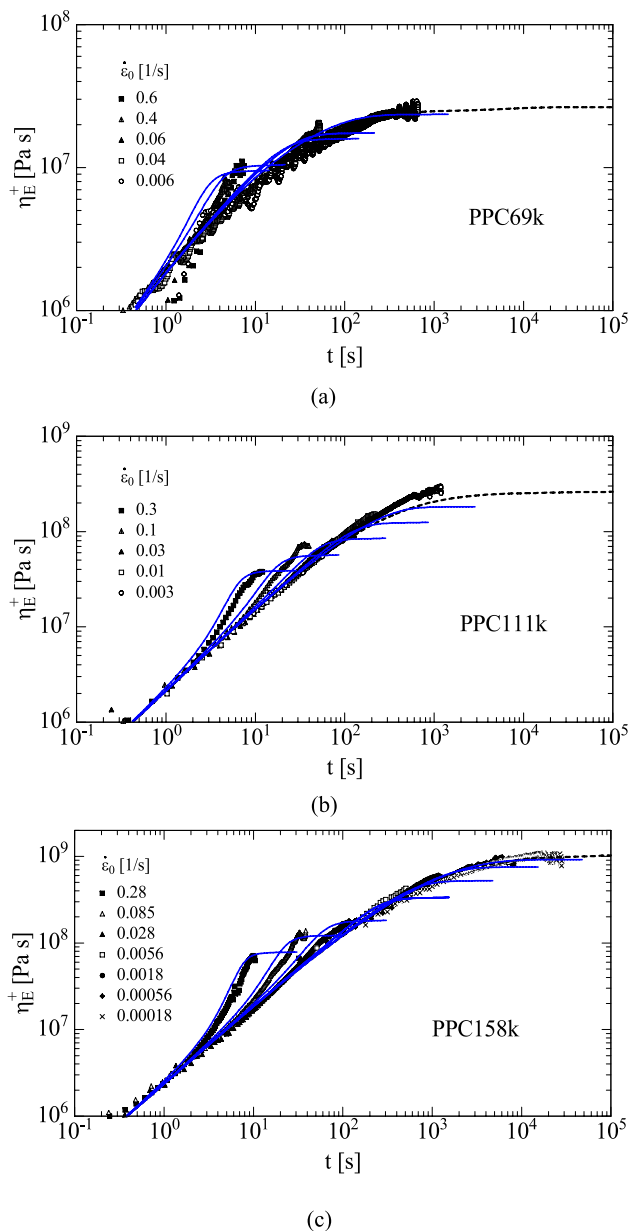


**Fig. 2** Comparison of experimental data of elongational stress growth coefficient  $\eta_E^+(t)$  (symbols) and predictions of the ERS model (full lines) at  $T=70$  °C. Symbols are the experimental data reported by Yang et al. (2022). Dotted lines indicate linear-viscoelastic elongational start-up viscosity

According to the Doi-Edwards model, the Rouse time  $\tau_R$ , the disengagement (or reptation) time  $\tau_d$  and the zero-shear viscosity  $\eta_0$  of monodisperse linear chains with  $Z$  entanglements are given by Dealy et al. (2018),

$$\tau_R = Z^2 \tau_e \quad (2)$$

$$\tau_d = 3Z \tau_R \quad (3)$$

$$\eta_0 = \frac{\pi^2}{12} G_N \tau_d \quad (4)$$

$\tau_e$  is the entanglement segment equilibration time. However, Eqs. (2), (3) and (4) neglect contour length fluctuation and constraint release effects (Dealy et al. 2018). In addition, as the polymers considered have polydispersities of 1.3 to 1.4, we identify here  $\tau_d$  with the mean quadratic average of the relaxation times of the discrete relaxation spectrum and calculate  $\eta_0$  from the discrete relaxation spectrum,

$$\tau_d = \frac{\sum_i g_i \tau_i^2}{\sum_i g_i \tau_i} \quad (5)$$

$$\eta_0 = \sum_i g_i \tau_i \quad (6)$$

For quantification of the Rouse time  $\tau_R$ , Osaki's approach (Osaki et al. 1982; Takahashi et al. 1993; Isaki et al. 2003; Menezes and Graessley 1982) is used, which extrapolates the Rouse time of unentangled polymer systems to the Rouse time of entangled polymer melts, and takes into account the power of 3.4 scaling of the zero-shear viscosity with molar mass  $M$ . This leads to the relation (Wagner 2014)

$$\tau_R = \frac{12M\eta_0}{\pi^2 \rho RT} \left( \frac{M_{cm}}{M} \right)^{2.4} \quad (7)$$

for the Rouse stretch relaxation time. As the polymer melts considered here feature polydispersities of 1.3 to 1.4, we identify  $M$  with  $M_w$  in Eq. (7).  $M_{cm}$  denotes the critical molar mass in the melt state, when the entanglement effect becomes apparent by a change of the power of 1 to power of 3.4 scaling of the zero-shear viscosity as a function of molar mass. For PPC, a value of  $M_{cm} = 2M_e = 11.8 \text{ kg/mol}$  and a density of  $1.26 \text{ kg/cm}^3$  was reported (Yang et al. 2021). For monodisperse polystyrene a value of  $M_{cm} = 35 \text{ kg/mol}$  has previously been used successfully for modelling of the transient and steady-state elongational and shear viscosities of well-entangled linear PS melts and solutions of linear PS (Wagner, 2014; Narimissa et al. 2020a,b, 2021; Wagner et al. 2021b,c). For PS520k, it is necessary to use a slightly higher value of  $M_{cm} = 38 \text{ kg/mol}$  in Eq. (9), resulting in  $\tau_R = 396 \text{ s}$  in order to obtain good agreement with the experimental elongational viscosity data. This may be due to the polydispersity of PS520k or inaccuracy of the nominal molecular weight of  $M_w = 520 \text{ kg/mol}$  as reported by the producer but is still within the accepted range of  $M_{cm} \cong 2\text{to}3M_{em}$ . The values of disengagement time, zero-shear viscosity, and stretch relaxation time, as calculated from Eqs. (5)–(7) and the plateau modulus  $G_N$ , as reported by Yang et al. (2021, 2022) are summarized in Table 1.

**Table 2** Relaxation spectra at reference temperature  $T_r$

PPC69k		PPC111k		PPC158k		PS520k	
$g_i$ [Pa]	$\tau_i$ [s]	$g_i$ [Pa]	$\tau_i$ [s]	$g_i$ [Pa]	$\tau_i$ [s]	$g_i$ [Pa]	$\tau_i$ [s]
3.16e+8	7.50e−6	3.11e+7	1.35e−4	2.46e+8	1.46e−5	1.21e+8	1.20e−4
5.24e+6	1.17e−4	9.95e+5	2.90e−3	1.73e+6	1.82e−3	2.28e+5	8.40e−2
8.42e+5	3.73e−3	3.49e+5	1.71e−2	3.67e+5	2.91e−2	7.14e+5	1.41e−2
1.67e+6	6.35e−4	1.45e+5	8.65e−2	1.43e+5	3.84e−1	1.01e+5	4.66e−1
3.49e+5	2.61e−2	1.04e+5	4.13e−1	1.47e+5	3.50e+0	3.84e+4	3.03e+0
2.19e+5	1.61e−1	1.08e+5	1.76e+0	1.87e+5	2.65e+1	2.68e+4	1.82e+1
2.17e+5	7.93e−1	1.29e+5	6.95e+0	2.20e+5	1.82e+2	2.95e+4	9.14e+1
2.36e+5	3.62e+0	1.65e+5	2.93e+1	1.65e+5	9.56e+2	3.57e+4	3.79e+2
1.93e+5	1.48e+1	1.79e+5	1.14e+2	2.26e+4	4.88e+3	5.03e+4	1.62e+3
8.22e+4	6.18e+1	8.73e+4	4.17e+2	4.13e+2	8.91e+4	4.88e+4	6.23e+3
8.46e+3	3.12e+2	1.15e+4	1.66e+3			2.92e+4	2.13e+4
9.12e+1	9.86e+3	2.36e+2	1.92e+4			8.87e+2	1.06e+5

### The enhanced relaxation of stretch (ERS) model and comparison to experimental data

#### ERS model equations

The ERS model is a special form of the molecular stress function (MSF) model, which is a generalized tube segment model with strain-dependent tube diameter (Wagner 1990; Narimissa and Wagner 2019). The extra stress tensor  $\sigma(t)$  of the MSF model is given by a history integral of the form

$$\sigma(t) \int_{-\infty}^t \frac{\partial G(t-t')}{\partial t'} f^2(t,t') S_{DE}^{IA}(t,t') dt' \tag{8}$$

$G(t)$  is the relaxation modulus, according to Eq. (1);  $t$  is the time of observation when the stress is measured, and  $t'$  indicates the time when a tube segment was created by reptation. The strain measure  $S_{DE}^{IA}$  represents the contribution to the extra stress tensor originating from the affine rotation of the tube segments, according to the “independent alignment (IA)” assumption of Doi and Edwards (1978a,b, 1979), and is given by

$$S_{DE}^{IA}(t,t') \equiv 5 \left\langle \frac{\mathbf{u}' \mathbf{u}'}{u'^2} \right\rangle_0 = 5S(t,t') \tag{9}$$

with  $S(t,t')$  being the relative- second order orientation tensor.  $\mathbf{u}' \mathbf{u}'$  is the dyad of a deformed unit vector  $\mathbf{u}' = \mathbf{u}'(t,t')$ ,

$$\mathbf{u}' \mathbf{F}_t^{-1} \cdot \mathbf{u} \tag{10}$$

$\mathbf{F}_t^{-1} = \mathbf{F}_t^{-1}(t,t')$  is the relative deformation gradient tensor, and  $u'$  is the length of  $\mathbf{u}'$ . The orientation average is indicated by  $\langle \dots \rangle_0$ ,

$$\langle \dots \rangle_0 \equiv \frac{1}{4\pi} \oint \dots \sin \theta_0 d\theta_0 d\varphi_0 \tag{11}$$

i.e. an average over an isotropic distribution of unit vectors  $\mathbf{u}$ .

$f = f(t,t')$  represents the inverse of the relative tube diameter  $a/a_0$ , and at the same time the relative length of a deformed tube segment Wagner and Narimissa (2021),

$$f(t,t') \frac{a_0}{a(t,t')} = \frac{l(t,t')}{l_0} \tag{12}$$

At time  $t=t'$  the tube segment was created with equilibrium tube diameter  $a_0$  and equilibrium length  $l_0$ . Equation (12) is a direct consequence of Eq. (A9) of Doi and Edwards (1978a), who showed that the line density  $n/l$ , i.e., the number  $n$  of monomer units of length  $b$  that are found per length  $l$  of the tube, is a well-defined thermodynamic quantity and defines the tube diameter  $a$  by the relation  $n/l = a/b^2$ . For  $f \equiv 1$ , Eq. (8) reduces to the original Doi-Edwards IA (DEIA) model.

$S_{DE}^{IA}$  is determined directly by the deformation history, according to Eq. (9), while  $f$  is found as solution of an evolution equation, considering affine tube segment deformation balanced by enhanced Rouse relaxation Wagner and Narimissa (2021). With increasing stretch and decreasing tube diameter  $a$ , the number of monomers in a control volume of length and diameter  $a$  will decrease with the consequence of enhanced relaxation of stretch in this control volume. The incremental increase of the relaxation rate with stretch is proportional to the 4th power of the stretch, and the relaxation rate therefore is proportional to the 5th power of the stretch. The evolution equation of the ERS model is obtained

as a balance of extension rate versus relaxation rate Wagner and Narimissa (2021),

$$\frac{\partial f}{\partial t} = f(\mathbf{K} : \mathbf{S}) - \frac{f^5 - 1}{5\tau_R} \quad (13)$$

with  $\mathbf{K}$  the deformation-rate tensor and initial condition  $f(t, t' = 0) = 1$ . Equations (8) and (13) represent the ERS model and are solved numerically.

In the limit of vanishing chain stretch, Eq. (13) degenerates naturally into the classical stretch evolution equation,

$$\frac{\partial f}{\partial t} = f(\mathbf{K} : \mathbf{S}) - \frac{1}{\tau_R}(f - 1) \quad (14)$$

with  $\tau_R = \frac{\zeta b^2 N^2}{3\pi^2 kT}$  being the Rouse stretch relaxation time. The classical assumption is that  $\zeta = \zeta_0$  is constant i.e. independent of deformation. The evolution Eq. (14) in combination with the stress tensor Eq. (8) leads to a diverging elongational viscosity  $\eta_E \rightarrow \infty$  as soon as the Weissenberg number  $Wi_R = \dot{\epsilon}\tau_R$  approaches a value of  $Wi_R = 1$ , see e.g. Wagner (2015).

Friction reduction models assume a decreasing monomeric friction coefficient  $\zeta$  with increasing orientation of chain segments resulting in an effective Rouse time

$$\tau_\zeta = \frac{\zeta b^2 N^2}{3\pi^2 kT} = \frac{\zeta}{\zeta_0} \tau_R \quad (15)$$

$\zeta_0$  is the friction coefficient at equilibrium. Consequently the stretch evolution Eq. (13) can then be expressed as

$$\frac{\partial f}{\partial t} = f(\mathbf{K} : \mathbf{S}) - \frac{1}{\tau_\zeta}(f - 1) = f(\mathbf{K} : \mathbf{S}) - \frac{\zeta_0}{\zeta} \frac{1}{\tau_R}(f - 1) \quad (16)$$

Comparison of Eqs. (13) and (16) leads to a normalized friction coefficient,

$$\frac{\zeta}{\zeta_0} = 5 \frac{f - 1}{f^5 - 1} \quad (17)$$

With  $f^5 - 1 = (f - 1)(f^4 + f^3 + f^2 + f + 1)$ , this results in (Wagner and Narimissa (2021)

$$\frac{\zeta}{\zeta_0} = \frac{5}{f^4 + f^3 + f^2 + f + 1} \quad (18)$$

The reduction of the stretch relaxation time with increasing stretch  $f$  and increasing tension in the chain can be represented by a monomeric friction coefficient  $\zeta = \zeta(f)$ , which reduces with increasing stretch, according to Eq. (18). Thus, the ERS model relates monomeric friction reduction quantitatively and parameter-free to chain segment stretch. In the perspective of the ERS model, monomeric friction reduction is the consequence of faster stretch equilibration of smaller

and smaller chain segments of diameter and length  $a = a_0/f$  with increasing stretch. On the other hand, as reviewed by Matsumiya and Watanabe (2021), friction reduction models are based on the assumption of monomeric friction being reduced by flow-induced coilignment of Kuhn segments, quantified by empirical correlations between friction coefficient and a suitable scalar measure of orientation. We remark that in these models, monomeric friction reduction might equally well be correlated with chain segment stretch as in the ERS model, because stretch and orientation are correlated by the orientation tensor  $\mathbf{S}$  in the evolution Eq. (16) of stretch. From this perspective, we may conclude that there is a common starting point of friction reduction models and the ERS model: It is the importance of faster stretch relaxation of smaller chain segments with increasing stretch.

### Comparison of ERS model predictions to experimental elongational flow data of PPC and PS

Figure 2 presents a comparison of the elongational stress growth coefficient  $\eta_E^+(t)$  of the three PPC melts considered with predictions of the ERS model. For PPC69k (Fig. 2a) the relaxation times  $\tau_i$  given in Table 2 had to be time-temperature shifted by a temperature factor  $a_T = 0.7$  in order to obtain agreement with the experimentally observed start-up viscosity. The discrepancy between predictions of the linear-viscoelastic start-up viscosities from SAOS versus VADER measurements was already noted by Masubuchi et al. (2022), as discussed below, and may be due to a small difference between the SAOS reference temperature and the VADER measurement temperature for PPC69. Overall and considering that the ERS model is exclusively based on the LVE characterization of the PPC melts, the agreement of data and model predictions for PPC69k (Fig. 2a) and PPC111k (Fig. 2b) can be rated as fair, for PPC158k (Fig. 2c) even as quantitative.

The comparison of the elongational stress growth coefficient  $\eta_E^+(t)$  of the PS520k melt with predictions of the ERS model is shown in Fig. 3. Again, agreement of data and model prediction is obtained within experimental accuracy.

The experimental data of the steady-state elongational viscosity  $\eta_E(\dot{\epsilon})$  as a function of strain rate  $\dot{\epsilon}$  and predictions of the ERS model for the three PPC melts investigated at  $T = 70^\circ\text{C}$  and the PS520k melt at  $T = 130^\circ\text{C}$  are shown in Fig. 4a. Within experimental accuracy, the agreement of data and model predictions can be rated as excellent. While the predictive capability of the ERS model has been shown earlier for nearly monodisperse PS melts (Wagner and Narimissa (2021)), it is remarkable that the polydispersity of the polymer melts considered here with values of 1.3 to 1.4 does not have a significant

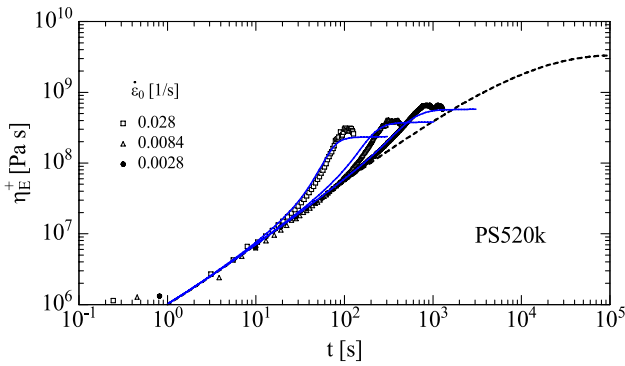


**Fig. 3** Comparison of experimental data of elongational stress growth coefficient  $\eta_E^+(t)$  (symbols) and predictions of the ERS model (full lines) for PS520k at  $T=130$  °C. Symbols are the experimental data reported by Yang et al. (2022). Dotted lines indicate linear-viscoelastic elongational start-up viscosity

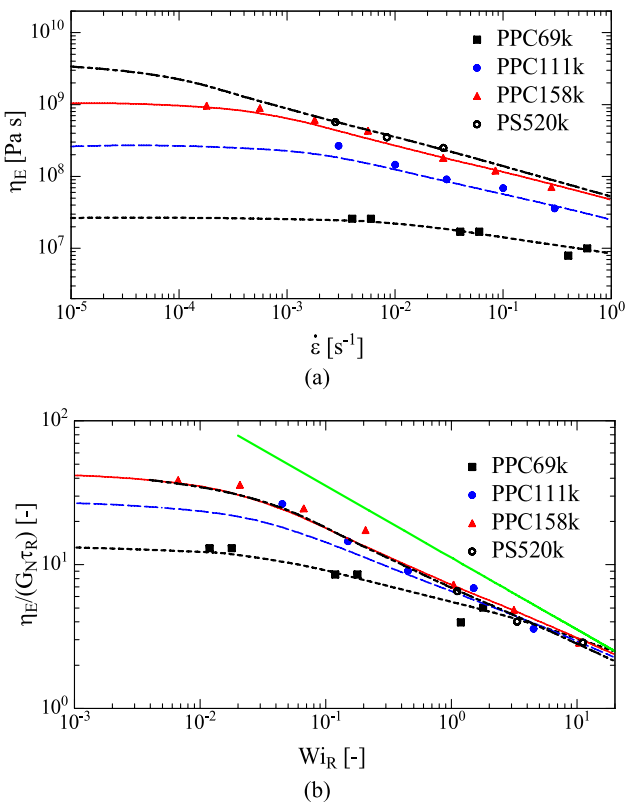


**Fig. 4 a** Comparison of experimental data of elongational viscosity  $\eta_E(\dot{\epsilon})$  (symbols) and predictions of the ERS model (lines) for PPC melts at  $T=70$  °C and PS520k melt at  $T=130$  °C. **b** Reduced elongational viscosity  $\eta_E/(G_N\tau_R)$  as a function of Weissenberg number  $Wi_R = \dot{\epsilon}\tau_R$ . Thick green straight line with slope of  $-1/2$  represents the asymptotic reduced elongational viscosity  $\frac{\eta_E}{G_N\tau_R} = 5\sqrt{5}Wi_R^{-1/2}$ .

effect. The effective “molecular weight average” Rouse time when calculated by Eq. (7) with  $M \equiv M_w$  seems to be sufficient as the characteristic parameter which determines chain stretch.

At high Weissenberg numbers  $Wi_R \equiv \dot{\epsilon}\tau_R$  and large stretch, when the steady state is reached and  $\partial f/\partial t = 0$ , the evolution Eq. (13) of the ERS model reaches the limit of  $f^2 = \sqrt{5}Wi_R$ , and the asymptotic tensile stress from Eq. (8) is given by  $\sigma = 5G_N f^2 = 5G_N\sqrt{5}Wi_R$ . As shown in Fig. 4b, the asymptotic reduced elongational viscosity  $\eta_E/(G_N\tau_R) = 5\sqrt{5}Wi_R^{-1/2}$  is approached at high  $Wi_R$ , while the experimental data feature a power-law slope, which is higher than  $-1/2$  and for well-entangled polymers closer to a value of  $-0.4$ , as already noted by Wagner et al. (2005). This is due to the broadness of the relaxation spectrum of even monodisperse polymers with the consequence that while the central part of the molecule with long relaxation times is increasingly orientated and stretched with increasing  $Wi_R$ , the chain ends with short relaxation times remain nearly isotropic. Figure 4 b is a temperature invariant representation of the data, which also highlights the importance of the Rouse time in the elongational thinning behaviour of polymer melts.

### PCN simulations and comparison to experimental data

#### PCN model and simulations

Because model and simulation scheme have been reported earlier (Masubuchi et al. 2001, 2014a, 2016), only a brief description shall be given below. In the primitive chain network (PCN) model, we replace an entangled polymer network with a slip-link network consisting of strands, nodes, and dangling ends. A polymer chain in the system corresponds to a path connecting a pair of dangling ends via strands. At each network node, a slip-link is located to bundle two segments according to the binary assumption of entanglement. The slip-links do not affect the sliding motion of the chain along the path, whereas they suppress the fluctuations in the perpendicular directions. A slip-link is removed when the bundled chain slides off at the chain end. Vice versa, a new slip-link is created at a dangling segment when it protrudes from the connected slip-link to hook another segment randomly chosen from the surrounding ones. The state variables of the system are the positions of slip-links and of dangling ends  $\{\mathbf{R}\}$ , the number of Kuhn segments assigned to network strands and dangling segments  $\{n\}$ , and the number of slip-links on each polymer chain  $\{Z\}$ . In the numerical simulation,  $\{\mathbf{R}\}$  obeys a Langevin-type equation of motion, in which the force balance is considered between the drag force, the tension acting on the connecting strands, the osmotic force suppressing density fluctuations, and the thermal random force. The time development of  $\{n\}$  is described

by a change-rate equation, in which the same force balance is considered as for  $\{\mathbf{R}\}$  but in 1-dimension along the chain. We trigger the change of  $\{Z\}$  by monitoring  $\{n\}$  at each dangling segment. When the value of  $n$  at an end segment falls below a certain critical value, we remove the connected slip-link and release the bundled segment. On the contrary, when  $n$  exceeds another critical value, we create a new slip-link on the subjected dangling segment to randomly hook a segment within a certain distance.

The simulation code employed in this study is the same as that utilized in the earlier studies (Yaoita et al. 2012; Masubuchi et al. 2014a, 2014b, 2021, 2022; Takeda et al., 2015), except that we consider here monomeric friction reduction, according to Eq. (18), as described later. The calculations are made according to non-dimensional quantities normalized by units of length, energy, and time. These units are chosen as the average strand length  $l_0$  under equilibrium conditions, the thermal energy  $k_B T$ , and the diffusion time of the single network node  $\tau_0 = 2n_0\zeta_0 l_0^2 / 6k_B T$ , where  $\zeta_0$  is the friction of the Kuhn segment at equilibrium, and  $n_0$  is the average number of Kuhn segments on the single strand. The factor of 2 stands for the fact that each network node consists of two strands.

Because the reduction of friction has no effect on the linear-viscoelastic response, the material parameters are the same as in the previous study (Masubuchi et al. 2022). The units of modulus  $G_0$ , molecular weight  $M_0$  and equilibration time  $\tau_0$  of a Kuhn segment were chosen as  $G_0 = 1.9$  (MPa),  $M_0 = 3.3$  (kg/mol), and  $\tau_0 = 7.8 \times 10^{-2}$  (s) for PPC melts at  $T = 70^\circ\text{C}$ , whereas  $G_0 = 0.55$  (MPa),  $M_0 = 11$  (kg/mol), and  $\tau_0 = 1.3$  (s) were used for the PS melt at  $T = 130^\circ\text{C}$ . Note that  $G_0$  and  $M_0$  are different from the plateau modulus  $G_N$  and the entanglement molecular weight  $M_e$ , as reported earlier (Yang et al. 2021, 2022). The difference is due to fluctuations imposed on network nodes in the PCN model (Masubuchi et al. 2003, 2020; Uneyama and Masubuchi 2021). Finite chain extensibility was considered with the maximum stretch  $\lambda_{\max}$  defined as  $\lambda_{\max} = \sqrt{n_K}$ , where  $n_K$  is the number of Kuhn segments on each strand on average. Determining the value of  $n_K$  from  $M_0$ , we chose  $\lambda_{\max} = 4.8$  for PPC, and  $\lambda_{\max} = 3.9$  for PS.

Concerning the change of friction, all the dynamics is accelerated when monomeric friction is reduced. Differently from the ERS model described above, not only the chain stretch and contraction, but also the segmental orientation and the entanglement rearrangement are affected by friction reduction. In the previous study (Masubuchi et al. 2022), the friction reduction model proposed by Ianniruberto et al. (2012) was used,

$$\frac{\zeta(S)}{\zeta_0} = \begin{cases} 1 & \text{for } S < S_c \\ (S/S_c)^{-\alpha} & \text{for } S \geq S_c \end{cases} \quad (19)$$

Here,  $\zeta$  is the monomeric friction coefficient,  $S$  is the average strand orientation defined as  $S = \langle u_x^2 \rangle - \langle u_y^2 \rangle$  with

the strand orientation vector  $\mathbf{u} = (u_x, u_y, u_z)$ .  $S_c$  and  $\alpha$  are empirical parameters that were chosen as  $S_c = 0.1$  and  $\alpha = 1.25$  (Masubuchi et al. 2022). In this study, we implemented the ERS friction reduction model of Eq. (18) for comparison by defining the stretch function  $f$  from Eq. (12) as the ratio of the average strand length  $\langle l \rangle$  under flow to the equilibrium strand length  $l_0$ ,

$$f = \frac{\langle l \rangle}{l_0} = \frac{\langle l \rangle}{b \langle \sqrt{n} \rangle} \quad (20)$$

Here,  $b$  is the Kuhn segment length, and  $\langle \sqrt{n} \rangle$  is the average square root of the number of Kuhn segments on each strand.

The simulations were conducted with periodic boundary conditions. We created 8 independent initial configurations in a flat simulation box with the dimensions of  $4 \times 45 \times 45$ . After sufficient equilibration, we stretched the system up to  $506 \times 4 \times 4$  corresponding to a maximum Hencky strain of 4.8 in order to obtain the elongational stress growth coefficient  $\eta_E^+(t)$ . The simulation box used is sufficiently large to accommodate the largest molecule with  $Z = 88$  as shown in the previous study (Masubuchi et al. 2022). Due to the nature of stochastic molecular simulations, the stress fluctuates over time and depends on the initial configuration. The magnitude of these inevitable uncertainties is discussed in the Appendix.

To account for the polydispersity of the melts, we assumed a distribution of molecular weights mimicking the polydispersity and the weight average molecular weight of the polymers considered, as presented in Table 3 and used in the previous study (Masubuchi et al. 2022). For comparison with the simulations for PPC158k, we also performed simulations with a monodisperse equivalent Z47 of PPC158k.

## Comparison of PCN simulations to experimental data of PPC and PS melts

Figure 5 shows the simulation results for the PPC melts. The simulation with constant friction (black dotted curves) clearly overestimates the experimental data (symbols), as reported previously (Masubuchi et al. 2022). If we employ the friction model proposed by Ianniruberto et al. (2012), Eq. (19) (red curves), the stress growth coefficient at high strain rates is reduced and approaches the experimental data. The simulation with the friction reduction resulting from the ERS model, Eq. (18) (blue curves), reproduces the data as well, even without any fitting parameter.

Note that the simulation entirely overestimates the data for PPC69k, although the linear viscoelasticity for this specific material has been semi-quantitatively reproduced (Masubuchi et al. 2022). As already mentioned, this discrepancy



**Table 3** Examined systems for PCN simulations

Code	Z	$\varphi_N^{\#}$	$Z_w$	$Z_w/Z_n$	$M_w^+$ (kg/mol)	$M_w/M_n^+$
PPC158k (PS520k)	11	0.09	47.3	1.31	158 (520)	1.30
	22	0.41				
	44	0.41				
	88	0.09				
PPC111k	8	0.09	33.7	1.30	111	1.30
	16	0.41				
	32	0.41				
	62	0.09				
PPC69k	4	0.1	20.6	1.41	68.8	1.43
	8	0.4				
	18	0.4				
	38	0.1				
Z47	47	1	47	1	-	-

<sup>#</sup>Number fraction of the chains

<sup>+</sup>Values reported according to GPC-MALS (Yang et al. 2021)

may be due to the time–temperature shift factor discussed above, and better agreement could be attained if  $\tau_0$  were optimized separately. Nevertheless, for consistency and direct comparison with the previous work (Masubuchi et al. 2022), we decided to use the same parameter set for the PCN simulations of all the PPC melts examined, as employed previously (Masubuchi et al, 2022).

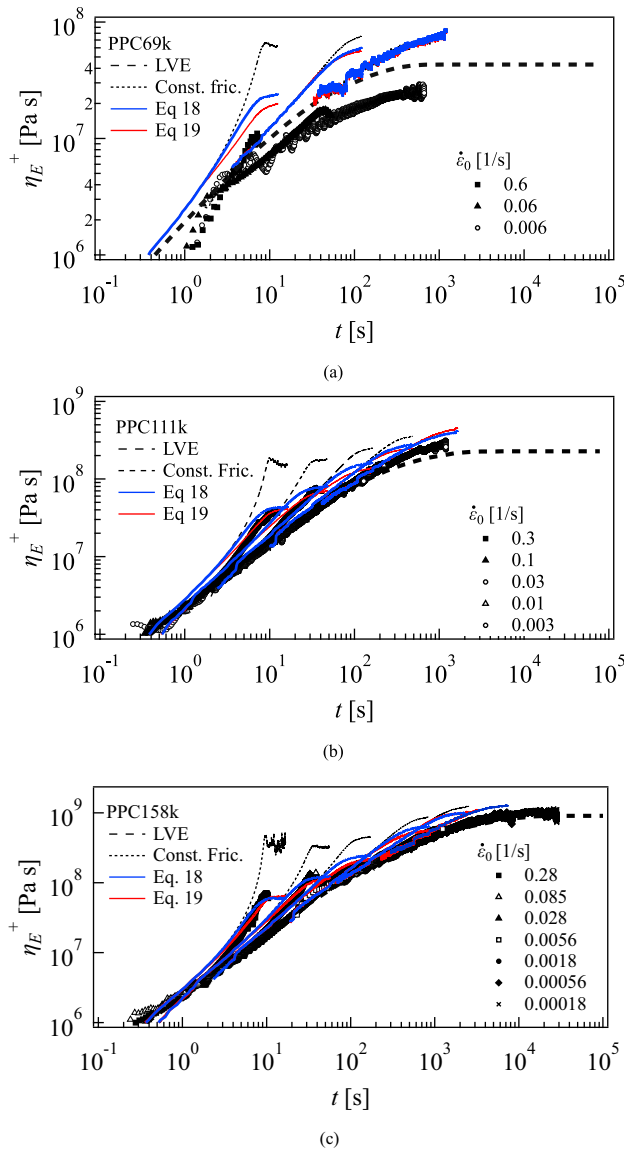
Figure 6 exhibits the simulation results for PS520k. This specific sample was chosen for comparison to PPC158k, and the average number of entanglements per chain and its polydispersity are almost identical to those of PPC158k. Thus, as shown in Table 3, the simulated system is the same as that of PPC158k, except for the maximum stretch ratio. However, the difference of  $\lambda_{\max}$  does not significantly affect the simulation result, which is essentially the same as that observed in Fig. 5 c.

Figure 7 shows the comparison between experimental data and PCN predictions for the steady-state elongational viscosity  $\eta_E(\dot{\epsilon})$ . As reported previously and shown in Figs. 5 and 6, the simulation with constant friction (black dotted curves) overestimates the data showing an upturn at a strain rate close to the contraction rate of the chains. In contrast, the experimental data do not exhibit such an upturn. Even at lower stretch rates than the critical rate for the upturn, the experimental data lie well below the prediction. They monotonically decrease with increasing strain rate when the strain rate is larger than the inverse of the longest relaxation time. The simulations with monomeric friction reduction capture this monotonically decreasing trend. The friction reduction models of Eqs. (18) (blue curves) and (19) (red curves) are in agreement with the experimental data both for the PPC melts (Fig. 7a) and for PS520k (Fig. 7b). Due to saturation of orientation at large strain rates, the simulation results using Eq. (19) show a trend to a certain constant lower-limited value of the viscosity for PPC 158 k, and deviate from the blue curve resulting from use of from Eq. (18), which shows a continued monotonic decrease. However, no experimental data are available at these high elongation rates.

Figure 8 a exhibits the friction change for PPC melts as a function of the strain rate. Equations (18) and (19) prescribe similar magnitudes of friction reduction, as reflected by the general agreement of the  $\eta_E(\dot{\epsilon})$  predictions. However, the strain rate dependence of the two friction models is qualitatively different from each other: The relative friction reduction resulting from Eq. (18) shows a monotonously decreasing trend, as it is inversely related to the increasing stretch with increasing strain rate. In contrast, Eq. (19) leads to concave curves with a decreasing slope at high elongation rates, in agreement with the increasing saturation of orientation at higher strain rates and the approach to a predicted lower-limited constant viscosity, as shown in Fig. 7. Experimental data at larger strain rates would be needed in order to decide on the importance of either saturation of orientation via the empirical expression of Eq. (19) or increasing stretch as expected by Eq. (18), on friction reduction.

Figure 8 b shows the reduction of the normalized average number of entanglements per chain plotted against the strain rate. For both simulations with friction reduction using Eqs. (18) and (19), the loss of entanglements is smaller, compared to the case with constant friction (shown by dotted black curves), reflecting that the effective strain rate is reduced by friction reduction, as reported earlier (Yaoita et al. 2012). Although the simulated losses of entanglements resulting from Eqs. (18) and (19) are rather similar, the effect of friction reduction on the loss of entanglements is also noticeable by comparison with Fig. 8a: Whenever the friction coefficient is lower, the loss of entanglements is smaller, and vice versa. Note that since the polymer systems examined have molecular weight distributions, the magnitude of the entanglement losses cannot be compared quantitatively to the case of monodisperse systems.

One may argue that the results may depend on the modeling of the molecular weight distribution. To discuss this issue, we conducted simulations for a monodisperse system, for which the molecular weight is assumed to be the same as the



**Fig. 5** Elongational stress growth coefficient  $\eta_E^+(t)$  of PPC melts in comparison to results of PCN simulations. Symbols are the experimental data reported by Yang et al. (2022). Dotted black curves are the simulation results with constant monomeric friction. Broken black curves are LVE envelopes. Blue and red solid curves are the simulation results for the friction models, according to Eqs. (18) and (19), respectively

weight average molecular weight  $M_w$  of PPC158k. The result is shown in Fig. 9. As reported previously, the polydispersity of  $M_w/M_n = 1.3$  does not strongly affect the simulation results, neither for constant friction nor for the friction reduction model, according to Eq. (19). A similar result is obtained here for the ERS friction reduction model of Eq. (18), and we conclude that the molecular weight distribution does not play any significant role in this case.

Another issue of the comparison between predictions of the tube-based ERS constitutive model and the PCN

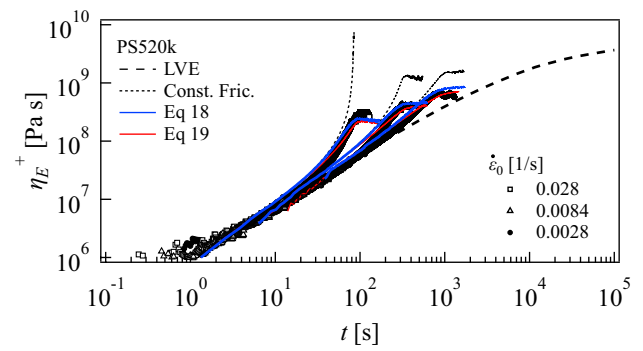


**Fig. 6** Elongational stress growth coefficient  $\eta_E^+(t)$  of PS520k in comparison to the results of PCN simulations. Symbols are the experimental data reported by Yang et al. (2022). Dotted black curves are the simulation results with constant monomeric friction. Broken black curves are LVE envelopes. Blue and red solid curves are the simulation results for the friction models according to Eqs. (18) and (19), respectively

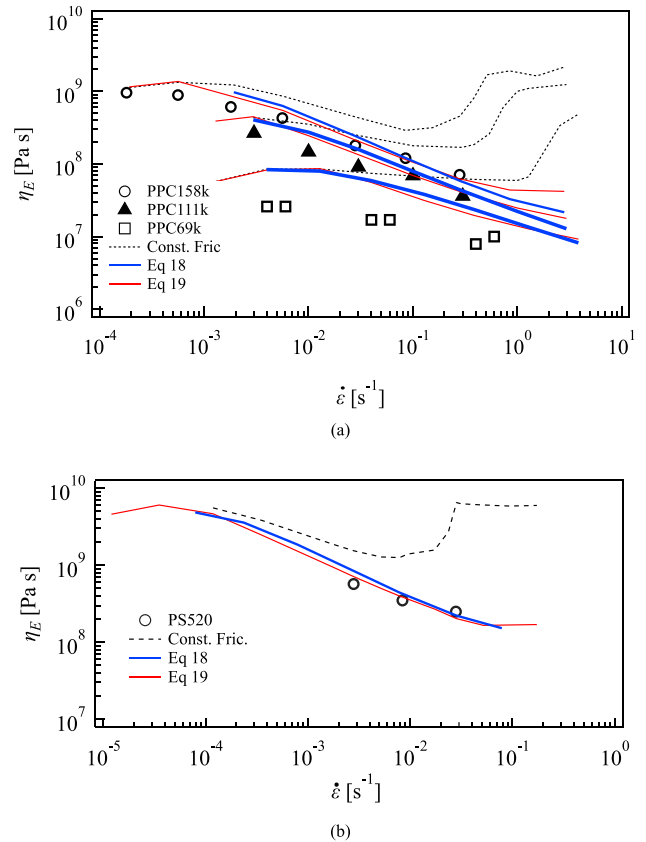


**Fig. 7** Steady-state elongational viscosity  $\eta_E$  as a function of elongation rate  $\dot{\epsilon}$  for PPC melts (a) and PS520k (b). Symbols are the experimental data by Yang et al. (2022). Broken, red solid and blue solid curves are the simulation results for constant friction, and the friction models, according to Eqs. (18) and (19), respectively

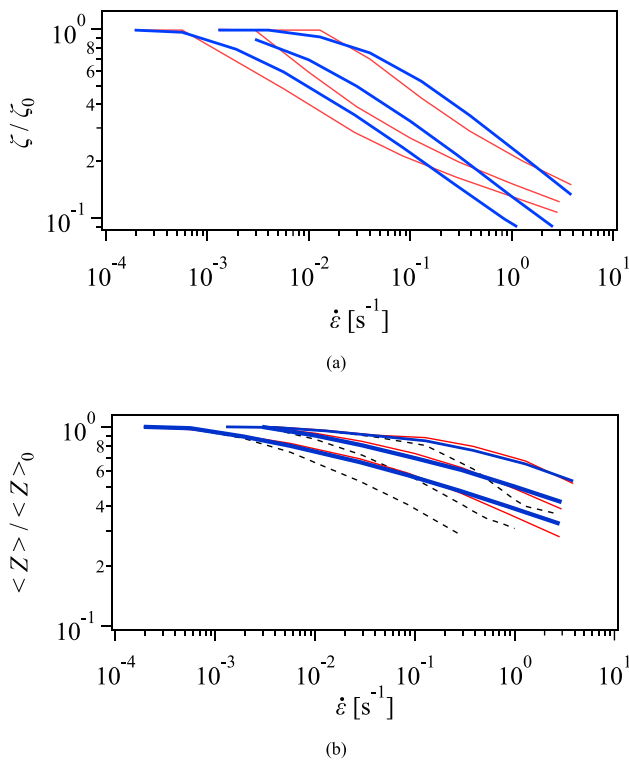


**Fig. 8** Strain-rate dependence of monomeric friction coefficient  $\zeta$  (a) and average number  $\langle Z \rangle$  of entanglements per chain (b) normalized by the equilibrium values for PPC 158 k, 111 k and 69 k, from left to right. Blue and red curves indicate the simulation results from Eqs. (18) and (19), respectively. Dotted black curves in (b) show the case without friction reduction

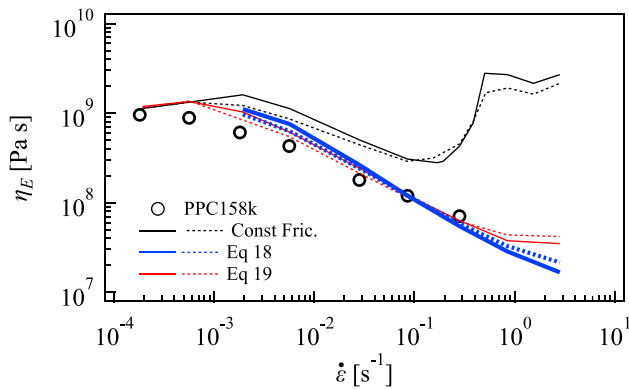


**Fig. 9** Steady-state elongational viscosity  $\eta_E$  as a function of elongation rate  $\dot{\epsilon}$  and the simulation results for the monodisperse (solid curves) and the polydisperse (dotted curves) case. Symbols are the experimental data by Yang et al. (2020) for PPC158k. Black, red, and blue curves are the simulation results for constant friction, and for the friction models, according to Eqs. (18) and (19), respectively

simulation is finite chain extensibility (FENE), which is implemented only in the simulation. Figure 10 shows the PCN simulation result for PPC158k without FENE, yet with the ERS friction reduction model, according to

Eq. (18). At large strain rates ( $\dot{\epsilon} \geq 0.5$  s<sup>-1</sup>), the simulation with FENE (dotted curve) shows a slight upward deviation from the simulation results obtained by assuming a Gaussian spring (solid curve). This upward trend results from the upper-limited chain stretch in the case of FENE. However, in the experimental window of strain rates investigated, FENE has no significant effect.

### Discussion and conclusions

We have shown that the ERS model is capable to predict the elongational viscosity data of the PPC melts as well as the PS melt considered, irrespective of whether the model is implemented as a mesoscopic tube-based constitutive equation or in the form of PCN simulation via a universal friction reduction model without any fitting parameter. To our knowledge, it is the first time that the equivalence of tube-based modelling and primitive chain network simulations has been shown. The accuracy of the PCN prediction is similar to the empirical friction reduction model proposed by Ianniruberto et al. (2012). The earlier friction models (Yaoita et al. 2012; Ianniruberto et al. 2012; Desai and Larson 2014) assume that friction is reduced by the oriented environment. The idea has been proven by atomistic molecular dynamics simulations for oligomers (Ianniruberto et al. 2012). However, it is unlikely that such highly oriented states are realized for entangled polymers at experimentally accessible stretch rates, which are typically smaller than the reciprocal entanglement segment time. In this respect, the ERS model with friction reduction being induced by chain stretch is worth of further investigation as a possible explanation of the phenomenon. The results of our investigations presented here imply that the physical mechanisms of

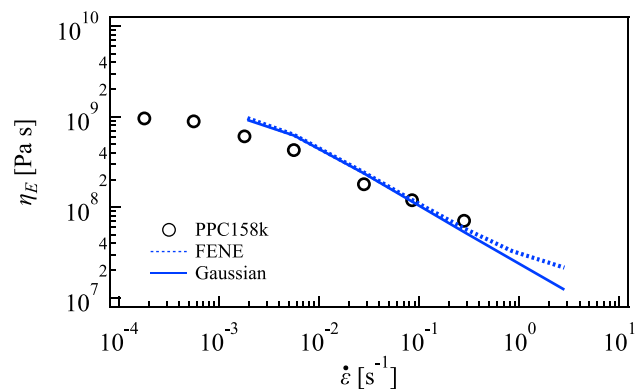


**Fig. 10** Steady-state elongational viscosity  $\eta_E$  as a function of elongation rate  $\dot{\epsilon}$  and the simulation results for Gaussian spring (solid curve) and FENE (dotted curve), both obtained with the ERS friction model of Eq. (18)

friction change are still controversial, at least in the case of entangled polymers.

Because there are no fitting parameters in Eq. (18), one may argue that the ERS friction reduction model cannot deal with the chemistry dependence of elongational behaviour of entangled polymer systems (Masubuchi 2014; Wingstrand et al., 2015). For this issue, we note that Eq. (18) implies indirectly a chemistry-dependent parameter, which is the maximum stretch implemented in the PCN simulation. Because the stretch  $f$  is upper-limited depending on the chemistry of the polymer chain, the magnitude of friction reduction is lower-limited (see Fig. 10). Although we did not see a significant difference in the simulation results between the PPC and the PS melt examined, we may observe such a saturation of stretch for stiff polymers. Alternatively, the effect of FENE could be implemented in the ERS model. We also note that for some polymers melts such as poly(*n*-butyl acrylate), hydrogen bonds may have significant effects on the elongational viscosity (Wagner et al. 2022), and we need to separately considering this from the possible effect of friction change.

Another line of future research will be the investigation of polymer solutions. Wagner and Narimissa (2021) have extended the ERS model to polymer solutions and considered the effect of polymer concentration. It will be interesting comparing mesoscopic tube-based modelling and PCN simulations for polymer solution data.

We also note that our implementation of the ERS friction reduction model in the PCN simulation is only one of the possible options. As mentioned above, in the present PCN implementation, we assume that friction reduction is affecting all the dynamics considered in the PCN simulation. In contrast, in the ERS model the accelerated motion due to friction reduction is exclusively considered for the chain sliding inside the tube, and orientational relaxation of the tube is not affected. In this sense, friction change for  $\{\mathbf{R}\}$  should be separately considered from that for  $\{n\}$  and  $\{Z\}$ . The other issue is the definition of the stretch function  $f$ . Note that the ERS model is a single segment model, in which the distribution of stretch along the chain is taken care of by the history integral of the deformation in Eq. (8). Although we define  $f$  for each entanglement segment in this PCN implementation, an alternative definition of  $f$  in the PCN model could be in terms the end-to-end vector of the chains. For the case of branched polymers,  $f$  will have to be separately considered for the backbone between branch points and branching arms Masubuchi et al. 2014b. Note also that we deal with multi-chain dynamics in the PCN simulations, and thus,  $f$  has a distribution among different chains. In particular, for the case with molecular weight distributions, the magnitude of stretch strongly depends on the molecular weight of mixed fractions, as reported earlier (Takeda et al. 2015). According to the concept of the ERS

model, we can calculate  $f$  for each component resulting in different values of monomeric friction. Even if we take an average value of  $f$ , there are several different possibilities for weighted averages. These issues have not been considered so far and are under investigation.

## Appendix

### Uncertainty of the PCN simulation results

Due to the nature of stochastic molecular simulations, the stress fluctuates over time and depends on the initial configuration. To demonstrate the magnitude of these inevitable uncertainties, we show in Fig. 11 the results of simulation runs starting from eight different initial configurations for both constant friction and the friction reduction model of Eq. (19). Apart from the simulation data at small strains ( $\epsilon < 1$ ) and small strain rates as demonstrated for  $\dot{\epsilon} = 0.03 \text{ s}^{-1}$  in Fig. 11, the fluctuations and their dependence on the initial configuration are negligible. The magnitude of the uncertainty at strains of  $\epsilon \geq 1$  is very small and is within the size of the symbols indicating the experimentally measured steady-state viscosity values in Figs. 7, 9, and 10. However, for the case of constant friction at high strain rates, conformational changes of fully-stretched FENE chains caused by stochastic hooking and unhooking between

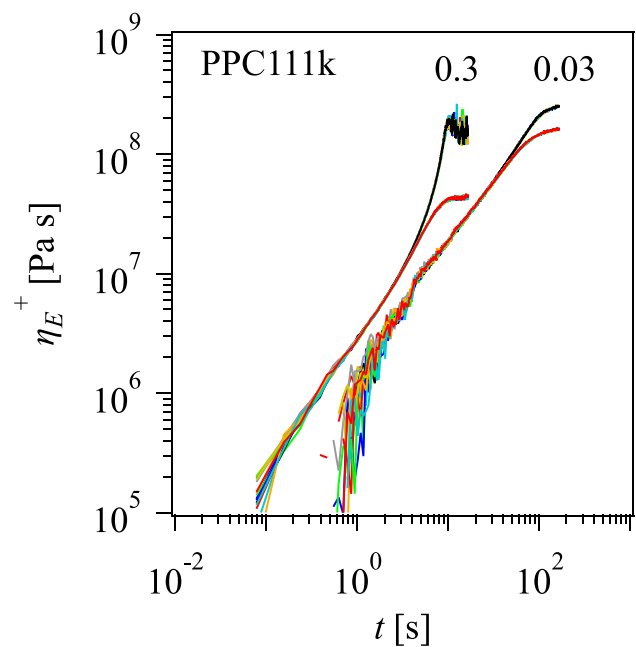


**Fig. 11** Elongational stress growth coefficient  $\eta_E^+(t)$  of PPC111k at strain rates of  $\dot{\epsilon} = 0.3$  and  $0.03 \text{ s}^{-1}$  obtained by PCN simulations with constant monomeric friction and the friction reduction model, according to Eq. (19). The simulation results of 8 independent initial configurations are indicated by different colours for each friction condition

different chains induce unavoidably large stress fluctuations at the steady state as seen in the upper curves for the strain rate of  $\dot{\epsilon} = 0.3s^{-1}$ .

**Acknowledgements** This work was partly supported by Grant-in-Aid for Scientific Research (B) No 22H01189 from Japan Society for the Promotion of Science (JSPS)

**Funding** Open Access funding enabled and organized by Projekt DEAL.

**Open Access** This article is licensed under a Creative Commons Attribution 4.0 International License, which permits use, sharing, adaptation, distribution and reproduction in any medium or format, as long as you give appropriate credit to the original author(s) and the source, provide a link to the Creative Commons licence, and indicate if changes were made. The images or other third party material in this article are included in the article's Creative Commons licence, unless indicated otherwise in a credit line to the material. If material is not included in the article's Creative Commons licence and your intended use is not permitted by statutory regulation or exceeds the permitted use, you will need to obtain permission directly from the copyright holder. To view a copy of this licence, visit <http://creativecommons.org/licenses/by/4.0/>.

## References

- Bach A, Rasmussen HK, Hassager O (2003a) Extensional viscosity for polymer melts measured in the filament stretching rheometer. *J Rheol* 47:429–441
- Bach A, Almdal K, Rasmussen HK, Hassager O (2003b) Elongational viscosity of narrow molar mass distribution polystyrene. *Macromolecules* 36:5174–5179
- Bhattacharjee PK, Oberhauser JP, McKinley GH, Leal LG, Sridhar T (2002) Extensional rheometry of entangled solutions. *Macromolecules* 35:10131–10148
- Bhattacharjee PK, Nguyen DA, McKinley GH, Sridhar T (2003) Extensional stress growth and stress relaxation in entangled polymer solutions. *J Rheol* 47:269–290
- Dealy JM, Read DJ, Larson RG (2018) Structure and rheology of molten polymers: from structure to flow behavior and back again. Carl Hanser Verlag GmbH Co KG, München, Germany
- Desai PS, Larson RG (2014) Constitutive model that shows extension thickening for entangled solutions and extension thinning for melts. *J Rheol* 58:255–279
- Doi M, Edwards SF (1978a) Dynamics of concentrated polymer systems. Part 2.- molecular motion under flow. *J Chem Soc, Faraday Trans* 74:1802–1817
- Doi M, Edwards SF (1978b) Dynamics of concentrated polymer systems. Part 3.- the constitutive equation. *J Chem Soc, Faraday Trans* 74:1818–1832
- Doi M, Edwards SF (1979) Dynamics of concentrated polymer systems. Part 4.- rheological properties. *J Chem Soc, Faraday Trans* 75:38–54
- Huang Q, Mednova O, Rasmussen HK, Alvarez NJ, Skov AL, Almdal K, Hassager O (2013a) Concentrated polymer solutions are different from melts: role of entanglement molecular weight. *Macromolecules* 46:5026–5035
- Huang Q, Alvarez NJ, Matsumiya Y, Rasmussen HK, Watanabe H, Hassager O (2013b) Extensional rheology of entangled polystyrene solutions suggests importance of nematic interactions. *ACS Macro Lett* 2:741–744
- Huang Q, Hengeller L, Alvarez NJ, Hassager O (2015) Bridging the gap between polymer melts and solutions in extensional rheology. *Macromolecules* 48:4158–4163
- Huang Q, Mangnus M, Alvarez NJ, Koopmans R, Hassager O (2016) A new look at extensional rheology of low-density polyethylene. *Rheol Acta* 55:343–350
- Ianniruberto G, Brasiello A, Marrucci G (2011) Friction coefficient does not stay constant in nonlinear viscoelasticity. In: *Proceedings 7th Ann. Eur. Rheol. Conf. Suzdal, Russia*, p 61–1
- Ianniruberto G, Marrucci G (2020) Molecular dynamics reveals a dramatic drop of the friction coefficient in fast flows of polymer melts. *Macromolecules* 53:2627–2633
- Ianniruberto G, Brasiello A, Marrucci G (2012) Simulations of fast shear flows of PS oligomers confirm monomeric friction reduction in fast elongational flows of monodisperse PS melts as indicated by rheoptical data. *Macromolecules* 45:8058–8066
- Ianniruberto G, Marrucci G, Masubuchi Y (2020) Melts of linear polymers in fast flows. *Macromolecules* 53:5023–5033
- Isaki T, Takahashi M, Urakawa O (2003) Biaxial Damping Function of Entangled Monodisperse Polystyrene Melts: Comparison with the Mead-Larson-Doi model. *J Rheology* 47:1201–1210
- Marrucci G, Ianniruberto G (2004) Interchain pressure effect in extensional flows of entangled polymer melts. *Macromolecules* 37:3934–3942
- Masubuchi Y (2014) Simulating the flow of entangled polymers. *Annu Rev Chem Biomol Eng* 5:11–33
- Masubuchi Y (2016) Molecular modeling for polymer rheology. In: *Reference module in materials science and materials engineering*. Elsevier, pp 1–7
- Masubuchi Y, Takimoto J-I, Koyama K et al (2001) Brownian simulations of a network of reptating primitive chains. *J Chem Phys* 115:4387–4394
- Masubuchi Y, Ianniruberto G, Greco F, Marrucci G (2003) Entanglement molecular weight and frequency response of sliplink networks. *J Chem Phys* 119:6925–6930
- Masubuchi Y, Yaoita T, Matsumiya Y, Watanabe H, Ianniruberto G, Marrucci G (2013) Stretch/orientation induced acceleration in stress relaxation in coarse-grained molecular dynamics simulations. *Nihon Reoroji Gakkaishi* 41:35–37
- Masubuchi Y, Matsumiya Y, Watanabe H (2014a) Test of orientation/stretch-induced reduction of friction via primitive chain network simulations for polystyrene, polyisoprene, and poly(*n*-butyl acrylate). *Macromolecules* 47:6768–6775
- Masubuchi Y, Matsumiya Y, Watanabe H et al (2014b) Primitive chain network simulations for Pom-Pom polymers in uniaxial elongational flows. *Macromolecules* 47:3511–3519
- Masubuchi Y, Doi Y, Uneyama T (2020) Entanglement molecular weight. *Nihon Reoroji Gakkaishi* 48:177–183
- Masubuchi Y, Ianniruberto G, Marrucci G (2021) Primitive chain network simulations of entangled melts of symmetric and asymmetric star polymers in uniaxial elongational flows. *Nihon Reoroji Gakkaishi* 49:171–178
- Masubuchi Y, Yang L, Uneyama T, Doi Y (2022) Analysis of elongational viscosity of entangled poly (propylene carbonate) melts by primitive chain network simulations. *Polymers* 14:741
- Matsumiya Y, Watanabe H (2021) Non-universal features in uniaxially extensional rheology of linear polymer melts and concentrated solutions: a review. *Prog Polymer Sci* 112:101325
- Menezes E, Graessley W (1982) Nonlinear rheological behavior of polymer systems for several shear-flow histories. *J Poly Sci Part b: Poly Phys* 20:1817–1833
- Narimissa E, Wagner MH (2019) Review on tube model based constitutive equations for polydisperse linear and long-chain branched polymer melts. *J Rheology* 63:361–375
- Narimissa E, Huang Q, Wagner MH (2020a) Elongational rheology of polystyrene melts and solutions: concentration dependence of the interchain tube pressure effect. *J Rheology* 64:95–110
- Narimissa E, Schweizer T, Wagner MH (2020b) A constitutive analysis of nonlinear shear flow. *Rheol Acta* 59:487–506

- Narimissa E, Poh L, Wagner MH (2021) Elongational viscosity scaling of polymer melts with different chemical constituents. *Rheol Acta* 60:163–174
- Osaki K, Nishizawa K, Kurata M (1982) Material time constant characterizing the nonlinear viscoelasticity of entangled polymeric systems. *Macromolecules* 15:1068–1071
- Poh L, Narimissa E, Wagner MH, Winter HH (2022) Interactive shear and extensional rheology - 25 years of IRIS Software. *Rheol Acta* 61:259–269
- Takahashi M, Isaki T, Takigawa T, Masuda T (1993) Measurement of biaxial and uniaxial extensional flow behavior of polymer melts at constant strain rates. *J Rheology* 37:827–846
- Takeda K, Sukumaran SK, Sugimoto M et al (2015) Primitive chain network simulations for elongational viscosity of bidisperse polystyrene melts. *Adv Model Simul Eng Sci* 2:11
- Uneyama T, Masubuchi Y (2021) Plateau moduli of several single-chain slip-link and slip-spring models. *Macromolecules* 54:1338–1353
- Wagner M, Narimissa E, Shabbir A (2022) Modelling the effect of hydrogen bonding on elongational flow of supramolecular polymer melts. *Rheol Acta* 61:637–647
- Wagner MH (1990) The nonlinear strain measure of polyisobutylene melt in general biaxial flow and its comparison to the Doi-Edwards model. *Rheol Acta* 29:594–603
- Wagner MH (2014) Scaling relations for elongational flow of polystyrene melts and concentrated solutions of polystyrene in oligomeric styrene. *Rheol Acta* 53:765–777
- Wagner MH (2015) An extended interchain tube pressure model for elongational flow of polystyrene melts and concentrated solutions. *J Non-Newtonian Fluid Mech* 222:121–131
- Wagner MH, Narimissa E (2021) A new perspective on monomeric friction reduction in fast elongational flows of polystyrene melts and solutions. *J Rheology* 65:1413–1421
- Wagner MH, Kheirandish S, Hassager O (2005) Quantitative prediction of transient and steady-state elongational viscosity of nearly monodisperse polystyrene melts. *J Rheology* 49:1317–1327
- Wagner MH, Narimissa E, Poh L, Shahid T (2021a) Modelling elongational viscosity and brittle fracture of polystyrene solutions. *Rheol Acta* 60:385–396
- Wagner MH, Narimissa E, Shahid T (2021b) Elongational viscosity and brittle fracture of bidisperse blends of a high and several low molar mass polystyrenes. *Rheol Acta* 60:803–817
- Wingstrand SL, Alvarez NJ, Huang Q, Hassager O (2015) Linear and nonlinear universality in the rheology of polymer melts and solutions. *Phys Rev Lett* 115:1–5
- Winter HH, Mours M (2006) The cyber infrastructure initiative for rheology. *Rheol Acta* 45:331–338
- Yang L, Uneyama T, Masubuchi Y, Doi Y (2021) Linear rheological properties of poly(propylene carbonate) with different molecular weights. *Nihon Reoroji Gakkaishi* 49:267–274
- Yang L, Uneyama T, Masubuchi Y, Doi Y (2022) Nonlinear shear and elongational rheology of poly(propylene carbonate). *Nihon Reoroji Gakkaishi* 50:127–135
- Yaoita T, Isaki T, Masubuchi Y, Watanabe H, Ianniruberto G, Marrucci G (2012) Primitive chain network simulation of elongational flows of entangled linear chains: stretch/orientation-induced reduction of monomeric friction. *Macromolecules* 45:2773–2782
- Ye X, Larson RG, Pattamaprom C, Sridhar T (2003) Extensional properties of monodisperse and bidisperse polystyrene solutions. *J Rheol* 47:443–468

**Publisher's note** Springer Nature remains neutral with regard to jurisdictional claims in published maps and institutional affiliations.